Contemporary Mathematics
https://ojs.wiserpub.com/index.php/CM/

Research Article

Synergistic Role of Ciliary Motion and Magnetohydrodynamics in Peristaltic Nanofluid Flow: Bio Applications

Zil-e-Huma[1], Niat Nigar[1], Nadeem Abbas[2*], M. Arslan Nazir[1], Wasfi Shatanawi[2]

[1] School of Mathematics & Statistics, Minhaj University Lahore, Lahore 54770, Pakistan
[2] Department of Mathematics and Sciences, College of Sciences and Humanities, Prince Sultan University, Riyadh 11586, Saudi Arabia
E-mail: nabbas@psu.edu.sa

Received: 14 October 2025; **Revised:** 14 November 2025; **Accepted:** 20 November 2025

Abstract: The synergistic interplay of ciliary motion and Magnetohydrodynamics (MHD) in facilitating the peristaltic transport of nanofluid presented a transformative approach for bio-applications. Our research enhanced medical diagnostics and increased the precision of drug delivery. Our analysis also examined the interactions between cilia-induced fluid motion and the influence of magnetic fields on nanofluid flow in a vertical endoscopic tube. A Mathematical model was created and solved through analytical as well as numerical procedures. We examined the impacts of involving factors on flow efficiency, heat transfer and particle dispersion. The results indicated that coordinated action of ciliary beating and magnetic field gradient significantly enhanced fluid propulsion and control. Our research indicated that combining ciliary mechanisms with an MHD-driven nanofluid system improved the movement of biofluid in a clinical situation. Magnetic force is observed to reduce velocity while buoyancy force tend to tends to increase it. A wider section of the tube exhibits a lower pressure gradient and facilitates smoother fluid flow with reduced resistance.

***Keywords*:** Magnetohydrodynamics (MHD), ciliary motion, nanofluid, peristaltic transport, vertical endoscopy tube

MSC: 34A45, 76A05, 76E30, 34B15

Nomenclature

$\overline{\overline{U}}$, $\overline{\overline{W}}$	Velocity profiles
$\overline{\overline{C}}$	Concentration
φ	Volume fraction of nanoparticles
N_b	Brownian motion parameter
N_t	Thermophoresis parameter
Q_0	Heat absorption
D_m	Molecular diffusivity
Re	Reynolds number
Gr	Grashof number
θ	Non-dimensional temperature

DOI: https://doi.org/10.37256/cm.7320268514

P	Pressure
μ	Dynamic viscosity
k	Thermal conductivity
ρ	Density

1. Introduction

Innovative methods are necessary to enhance efficiency and precision due to the complex dynamics of biofluid transport in constrained biological systems. Ciliary motion refers to the synchronized beating of hair-like structures and is a natural mechanism essential for enabling fluid passage in biological channels. Such approaches combine the unique thermophysical characteristics of nanofluids with concepts from Magnetohydrodynamics (MHD), utilizing magnetic fields to influence electrically conductive fluids.

Fatima and Asghar [1] examined the dynamics of fluid flow resulting from a pressure gradient generated by peristaltic waves. Tanveer et al. [2] conducted a theoretical analysis of peristaltic blood flow for a non-Newtonian fluid influenced by MHD effects. Javid et al. [3] studied biofluid peristaltic motion within a divergent complex wavy channel. Elboughdiri et al. [4] investigated peristaltic pumping of hybrid nanofluid with magnetic device effects for applications in human endoscopy. Devakar et al. [5] analyzed magnetohydrodynamic effects on the peristaltic flow of couple stress fluid in an inclined tube with endoscope effects. Asha et al. [6] examined entropy generation and radiation effects in hyperbolic tangent fluid with hybrid nanoparticles during peristaltic transport through an endoscope.

The Sisko fluid model represents an important non-Newtonian framework describing stress-strain behavior and is widely applied in hydrodynamic systems to reduce friction. Jawad et al. [7] explored magnetic field effects on Sisko nanofluid thin film flow over a stretching surface. McCash et al. [8] investigated chemical reaction and activation energy effects in Sisko fluid over a curved surface. Shaheen and Asjad [9] studied the peristaltic flow of Sisko fluid with viscous dissipation over a convectively heated surface.

MHD examines the flow behavior of conducting fluids under magnetic phenomena, focusing on the interaction between magnetic fields and electrically conductive fluids. Mumtaz et al. [10] performed a thermal performance analysis of quaternary hybrid nanofluid considering radiative and Joule heating effects. Alharbi et al. [11] provided exact solutions for non-Newtonian blood flow with nanoparticles in porous arteries. Kumar et al. [12] utilized artificial neural networks for mass transfer and bioconvection analysis in radiative Eyring-Powell flow. Arshad [13] analyzed MHD hybrid nanofluid flow in a rotating system with thermal radiation effects. Ayub et al. [14] discussed biological interactions between microswimmers and cross fluid with inclined MHD effects. Tanveer and Ashraf [15] investigated mixed convection flow of Sisko nanofluid with entropy generation and Joule heating. Bahnasy and Abdel-Wahab [16] developed a mathematical model for suspension fluid flow under flexible endoscopy effects.

Rafiq et al. [17] evaluated activation energy and variable property effects on peristaltic flow through a porous wall channel. Abbas et al. [18] examined the peristaltic transport of Casson fluid in a non-uniform inclined tube using Rosseland approximation. Hafez et al. [19] studied MHD peristaltic transport of Casson fluid on an inclined plane. Mahendra et al. [20] performed entropy analysis on bioconvective peristaltic flow involving gyrotactic microorganisms in an Eyring-Powell nanofluid. Abdelhafez et al. [21] investigated magnetic field effects on blood peristaltic flow in an asymmetric channel. Alhazmi et al. [22] studied thermal convection in nanofluid for peristaltic flow in a nonuniform channel. Fatima et al. [23] explored electro-osmotic and thermal energy influences in tri-hybrid nanofluid for artificial olfactory cilia. Asghar et al. [24] analyzed the Ellis fluid model in a complex divergent channel, emphasizing rheological characterization for flow stability prediction. Sadaf et al. [25] developed a mathematical model for cross-fluid motion in a peristaltic channel with viscous dissipation and MHD effects. Asghar et al. [26] investigated the electro-fluid-dynamic behavior of soft-bodied organisms navigating mucus with diverse rheological properties, providing insights into bio-propulsion in nonlinear viscous environments.

The investigation of a biorheological fluid within the context of electro-magneto-hydrodynamics is examined from a theoretical perspective and utilized external fields of electricity and magnetism in fluid mechanics. MHD directly converts heat energy into electrical energy without involving mechanical processes. Our objective is to introduce an approach

for an MHD Prandtl fluid. By varying the material parameters, the Prandtl fluid exhibited a range of characteristics, particularly in the context of non-Newtonian fluid, which justifies its consideration. The nanofluid model of peristaltic flow in a vertical endoscopic tube has not yet detonated. As a result, we have emphasized the peristaltic flow of nanofluid in a vertical endoscopic tube in the current study. A model of the two-dimensional nanofluid governing equations in a vertical endoscopic tube that takes curvature into account is created. The simplified highly nonlinear partial differential equation is solved analytically using the homotopy perturbation method, following nondimensionalization and with the assumptions of the long wavelength and low Reynolds number approximation. Finally, graphs are plotted to discuss the physical phenomena.

2. Mathematical formulation

In a vertical endoscopic tube, evaluate the non-Newtonian Prandtl nanofluid peristaltic flow. The flow is driven by sinusoidal waves moving on the tube walls at a constant velocity. The flow pattern of the configuration is presented in Figure 1. The outer tube features sinusoidal waves on its wall, maintaining a constant temperature and the inner device is rigidly held at an exact temperature. The wall surface geometry is given as follows:

$$\bar{\bar{R}}_1 = b_1,$$

$$\bar{\bar{R}}_2 = b_2 + e\sin\frac{2\pi}{\lambda}\left(\bar{\bar{Z}} - c_1\bar{\bar{t}}\right).$$

Where e is a wave's amplitude, λ is a wave length, c_1 is the speed of waves, $\bar{\bar{t}}$ is the time, and b_1 and b_2 are the outer and inner tube radii, respectively.

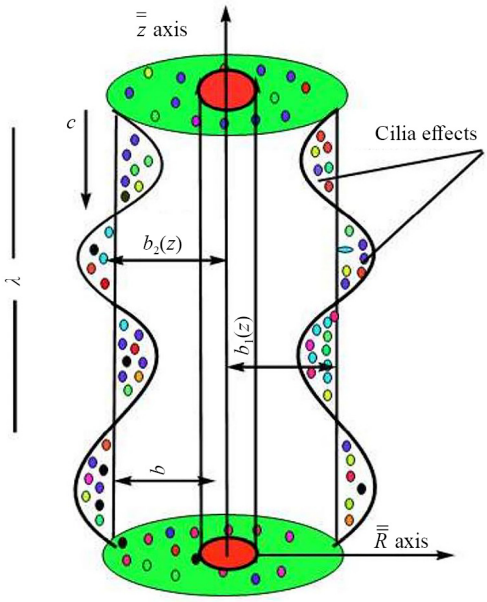

Figure 1. Physical phenomenon model

With the transformation create a wave element $(\bar{\bar{r}}, \bar{\bar{z}})$ that is moving away from the constant frame $(\bar{\bar{R}}, \bar{\bar{Z}})$ with velocity c_1,

$$\bar{\bar{Z}} = \bar{\bar{Z}} - c_1\bar{\bar{t}}, \quad \bar{\bar{r}} = \bar{\bar{R}}, \quad \bar{\bar{w}} = \bar{\bar{W}} - c_1, \quad \bar{\bar{u}} = \bar{\bar{U}}.$$

The cilia tips' mathematical equation is provided in the manner

$$\bar{\bar{R}} = \bar{\bar{h}} = \bar{\bar{F}}(\bar{\bar{Z}}, \bar{\bar{t}}) = \left[a + ba\cos\left(\frac{2\pi}{\lambda}\right)(\overline{\overline{z1}} - c\bar{\bar{t}})\right],$$

$$\bar{\bar{Z}} = \bar{\bar{G}}\left(\overline{\overline{Z1}}, \bar{\bar{Z}}_2, t\right) = \bar{\bar{Z}}_1 + \epsilon\alpha b\cos\left(\frac{2\pi}{\lambda}\right)(\overline{\overline{z1}} - c\bar{\bar{t}}).$$

Ciliated tube radius is a wavelength represented by λ. ϵ is the mean Wave speed. Non-dimensional metric concerning cilia is represented by c. Elliptic motion of tips of cilia is measured by eccentricity, which is represented by α. Velocities caused by cilia tips are mathematically written as

$$\overline{\overline{W}} = \frac{\partial\bar{\bar{z}}}{\partial\bar{\bar{t}}}\bigg| Z_o = \frac{\partial\bar{\bar{h}}}{\partial\bar{\bar{t}}} + \frac{\partial\bar{\bar{h}}}{\partial\bar{\bar{z}}}\cdot\frac{\partial\bar{\bar{z}}}{\partial\bar{\bar{t}}} = \frac{\partial\bar{\bar{s}}}{\partial\bar{\bar{t}}} + \frac{\partial\bar{\bar{s}}}{\partial\bar{\bar{x}}}\overline{\overline{W}},$$

$$\overline{\overline{U}} = \frac{\partial\bar{\bar{r}}}{\partial\bar{\bar{t}}}\bigg| Z_o = \frac{\partial\bar{\bar{f}}}{\partial\bar{\bar{t}}} + \frac{\partial\bar{\bar{f}}}{\partial\bar{\bar{z}}}\cdot\frac{\partial\bar{\bar{z}}}{\partial\bar{\bar{t}}} = \frac{\partial\bar{\bar{h}}}{\partial\bar{\bar{t}}} + \frac{\partial\bar{\bar{h}}}{\partial\bar{\bar{x}}}\overline{\overline{W}},$$

$$\overline{\overline{W}} = -\frac{\left(\frac{4\pi}{2\lambda}\right)\left(\epsilon\mathrm{Bab}\sin\left(\frac{4\pi}{2\lambda}\right)(\bar{\bar{z}} - c\bar{t})\right)}{1 - \left(\frac{4\pi}{2\lambda}\right)\left(\epsilon\alpha ac\cos\left(\frac{4\pi}{2\lambda}\right)(\bar{\bar{z}} - c\bar{t})\right)} = \bar{\bar{x}}(\overline{\overline{z1}}, \bar{\bar{t}}),$$

$$\overline{\overline{U}} = -\frac{\left(\frac{4\pi}{2\lambda}\right)\left(\epsilon\mathrm{Bab}\cos\left(\frac{4\pi}{2\lambda}\right)(\overline{\overline{z1}} - c1\bar{\bar{t}})\right)}{1 - \left(\frac{4\pi}{2\lambda}\right)\left(\epsilon\alpha ac\cos\left(\frac{2\pi}{\lambda}\right)(\bar{\bar{z}} - c\bar{\bar{t}})\right)} \quad \text{at} \quad \bar{\bar{r}} = \bar{\bar{H}}.$$

Following are the basic equations for momentum, continuity, and nanoparticle concentrations: [9]

$$\frac{\partial\bar{\bar{U}}}{\partial\bar{\bar{R}}} + \frac{\bar{\bar{U}}}{\bar{\bar{R}}} + \frac{\partial\overline{\overline{W}}}{\partial\bar{\bar{Z}}} = 0 \tag{1}$$

$$\rho\left(\frac{\partial}{\partial\bar{\bar{t}}} + \bar{\bar{u}}\frac{\partial}{\partial\bar{\bar{R}}} + \overline{\overline{W}}\frac{\partial}{\partial\bar{\bar{Z}}}\right)\bar{\bar{u}} = -\frac{\partial\bar{\bar{P}}}{\partial\bar{\bar{r}}} + \frac{1}{\bar{\bar{r}}}\frac{\partial}{\partial\bar{\bar{r}}}\left(r\bar{\bar{S}}_{\bar{r}\bar{r}}\right) + \frac{\partial}{\partial\bar{\bar{Z}}}\left(\bar{\bar{S}}_{\bar{r}\bar{Z}}\right) - \frac{\bar{\bar{S}}_{\bar{\theta}\bar{\theta}}}{\bar{\bar{r}}}$$

$$\rho\left(\frac{\partial}{\partial\bar{\bar{t}}} + \bar{\bar{u}}\frac{\partial}{\partial\bar{\bar{R}}} + \overline{\overline{W}}\frac{\partial}{\partial\bar{\bar{Z}}}\right)\overline{\overline{W}} = -\frac{\partial\bar{\bar{P}}}{\partial\bar{\bar{Z}}} + \frac{1}{\bar{\bar{r}}}\frac{\partial}{\partial\bar{\bar{R}}}\left(\bar{\bar{r}}\bar{\bar{S}}_{\bar{r}\bar{r}}\right) + \frac{\partial}{\partial\bar{\bar{Z}}}\left(\bar{\bar{S}}_{\bar{r}\bar{Z}}\right) + \rho g\alpha\left(\bar{\bar{T}} - \bar{\bar{T}}_0\right) + \rho g\alpha\left(\bar{\bar{C}} - \bar{\bar{C}}_0\right) - \sigma B_0^2\overline{\overline{W}}$$

$$\rho c_p\left(\frac{\partial}{\partial\bar{\bar{t}}}+\bar{\bar{U}}\frac{\partial}{\partial\bar{\bar{r}}}+\bar{\bar{W}}\frac{\partial}{\partial\bar{\bar{Z}}}\right)\bar{\bar{T}}=\bar{\bar{S}}_{rr}\frac{\partial\bar{\bar{U}}}{\partial\bar{\bar{r}}}+\bar{\bar{S}}_{\bar{R}\bar{Z}}\frac{\partial\bar{\bar{W}}}{\partial\bar{\bar{r}}}+\bar{\bar{S}}_{\bar{r}\bar{Z}}\frac{\partial\bar{\bar{U}}}{\partial\bar{\bar{Z}}}+\bar{\bar{S}}_{\bar{Z}\bar{Z}}\frac{\partial\bar{\bar{U}}}{\partial\bar{\bar{r}}}+\bar{\bar{S}}_{\bar{\theta}\bar{\theta}}\bar{\bar{U}}+\bar{\bar{r}}\left(\frac{\partial^2\bar{\bar{T}}}{\partial\bar{\bar{r}}^2}+\frac{1}{\bar{\bar{R}}}\frac{\partial\bar{\bar{T}}}{\partial\bar{\bar{r}}}+\frac{\partial^2\bar{\bar{T}}}{\partial\bar{\bar{Z}}^2}\right) \tag{2}$$

$$\left(\frac{\partial}{\partial\bar{\bar{t}}}+\bar{\bar{U}}\frac{\partial}{\partial\bar{\bar{R}}}+\bar{\bar{W}}\frac{\partial}{\partial\bar{\bar{Z}}}\right)\bar{\bar{C}}=D\left(\frac{\partial^2\bar{\bar{C}}}{\partial\bar{\bar{r}}^2}+\frac{1}{\bar{\bar{R}}}\frac{\partial\bar{\bar{C}}}{\partial\bar{\bar{r}}}+\frac{\partial^2\bar{\bar{C}}}{\partial\bar{\bar{Z}}^2}\right)+\frac{D\bar{\bar{k}}_T}{\bar{\bar{T}}_0}\left(\frac{\partial^2\bar{\bar{T}}}{\partial\bar{\bar{r}}^2}+\frac{1}{\bar{\bar{r}}}\frac{\partial\bar{\bar{T}}}{\partial\bar{\bar{r}}}+\frac{\partial^2\bar{\bar{T}}}{\partial\bar{\bar{Z}}^2}\right).$$

The associated boundary conditions on the wave frame are:

$$\begin{aligned}
&\bar{\bar{w}}=-c_1,\ \bar{\bar{T}}=\bar{\bar{T}}_0,\ \bar{\bar{C}}=\bar{\bar{C}}_0,\\
&\bar{\bar{w}}=-c_1,\ \text{at}\ \ \bar{\bar{r}}=\bar{\bar{r}}_1\\
&\bar{\bar{T}}=\bar{\bar{T}}_1,\ \bar{\bar{C}}=\bar{\bar{C}}_1,\ \text{at}\ \ \bar{\bar{r}}=\bar{\bar{r}}_2=a_2+e\sin\frac{2\pi}{\lambda}(\bar{\bar{Z}}).
\end{aligned} \tag{3}$$

The non-dimensional variables that follow:

$$Z=\frac{\bar{Z}}{\lambda},\quad Z=\frac{\bar{\bar{z}}}{\lambda},\quad R=\frac{\bar{\bar{R}}}{a_2},\quad r=\frac{\bar{\bar{r}}}{a_2},\quad W=\frac{\bar{\bar{W}}}{c_1},\quad w=\frac{\bar{\bar{w}}}{c_1},$$

$$U=\frac{\lambda\bar{\bar{U}}}{a_2c_1},\quad u=\frac{\lambda\bar{\bar{u}}}{a_2c_1},\quad P=\frac{a_2^2\bar{\bar{P}}}{c_1\lambda},\quad \theta=\frac{\left(\bar{\bar{T}}-\bar{\bar{T}}_1\right)}{\left(\bar{\bar{T}}_0-\bar{\bar{T}}_1\right)},\quad t=\frac{c_1\bar{\bar{t}}}{\lambda},$$

$$\delta=\frac{a_2}{\lambda},\quad Re=\frac{\rho c_1a_2}{\mu},\quad \sigma=\frac{\left(\bar{\bar{C}}-\bar{\bar{C}}_1\right)}{\left(\bar{\bar{C}}_0-\bar{\bar{C}}_1\right)},\quad r_2=\frac{\bar{\bar{r}}_2}{a_2}=1+\varphi\sin(2\pi z),$$

$$\alpha=\frac{k}{(\rho c)_f},\quad N_t=\frac{(\rho c)_pD_{\bar{T}}\left(\bar{\bar{C}}_0-\bar{\bar{C}}_1\right)}{(\rho c)_{f\alpha}},\quad N_b=\frac{(\rho c)_pD_B\left(\bar{\bar{C}}_0-\bar{\bar{C}}_1\right)}{(\rho c)_f},$$

$$M=\sqrt{\frac{\sigma}{\mu}}B_0\alpha,\quad G_r=\frac{g\alpha a_2^3\left(\bar{\bar{T}}_0-\bar{\bar{T}}_1\right)}{\nu^2},\quad B_r=\frac{g\alpha a_2^3\left(\bar{\bar{C}}_0-\bar{\bar{C}}_1\right)}{\nu^2}. \tag{4}$$

Where the parameters of thermophoresis, Brownian motion, Grashof number, and Brinkman number are, respectively, N_b, N_t, G_r and B_r.

With the help of the Equation (5) when Equations (1) to (4), a simplified equations are:

$$\frac{\partial u}{\partial r}+\frac{u}{r}+\frac{\partial w}{\partial z}=0 \tag{5}$$

$$\frac{\partial P}{\partial r} = 0 \tag{6}$$

$$\frac{\partial P}{\partial z} = \frac{1}{r}\frac{\partial}{\partial r}(rS_{rz}) + G_r\theta + B_r\sigma - M^2(w+1) \tag{7}$$

$$\frac{1}{r}\frac{\partial}{\partial r}\left(r\frac{\partial \theta}{\partial r}\right) + N_b\frac{\partial \theta}{\partial r}\frac{\partial \sigma}{\partial r} + N_t\left(\frac{\partial \theta}{\partial r}\right)^2 = 0 \tag{8}$$

$$\frac{1}{r}\frac{\partial}{\partial r}\left(r\frac{\partial \sigma}{\partial r}\right) + \frac{N_t}{N_b}\left(\frac{1}{r}\frac{\partial}{\partial r}\left(r\frac{\partial \theta}{\partial r}\right)\right) = 0. \tag{9}$$

Where $\bar{S}_{\bar{r}\bar{z}} = \alpha\left(\frac{\partial \bar{w}}{\partial \bar{r}}\right) + \beta\left(\frac{\partial \bar{w}}{\partial \bar{r}}\right)^3$.
Using Equation (7) and the value of $\bar{S}_{\bar{r}\bar{z}}$

$$\frac{\partial \bar{P}}{\partial \bar{z}} = \frac{1}{r}\frac{\partial}{\partial r}\left(r\left(\alpha\left(\frac{\partial \bar{w}}{\partial \bar{r}}\right) + \beta\left(\frac{\partial \bar{w}}{\partial \bar{r}}\right)^3\right)\right) + G_r\theta + B_r\sigma - M^2(w+1). \tag{10}$$

3. Approximations by homotopy perturbation

To the analytical solution for velocity, the homotopy perturbation approach is applied.

$$H(q, w) = L(w) - L(W_{10}) + qL(W_{10}) + q\left[\frac{1}{r}\frac{\partial}{\partial r}\left(r\left(\alpha\left(\frac{\partial \bar{w}}{\partial \bar{r}}\right) + \beta\left(\frac{\partial \bar{w}}{\partial \bar{r}}\right)^3\right)\right) + G_r\theta + B_r\sigma - \frac{\partial P}{\partial z} - M^2(w+1)\right]$$

$$L(w) = L(W_{10}) - qL(W_{10}) - q\left[\frac{1}{r}\frac{\partial}{\partial r}\left(r\left(\alpha\frac{\partial \bar{w}}{\partial \bar{r}} + \beta\left(\frac{\partial \bar{w}}{\partial \bar{r}}\right)^3\right)\right) + G_r\theta + B_r\sigma - \frac{\partial P}{\partial z} - M^2(w+1)\right]. \tag{11}$$

Here, L is the linear machinist, and $L = \frac{1}{R}\frac{\partial}{\partial R}\left(R\frac{\partial}{\partial R}\right)$ and $q \in [0, 1]$ is a parameter in embedding.
Let us define:

$$w = w_0 + qw_1 + q^2w_2 + \cdots$$

$$P = P_1 + qP_2 + q^2P_3 + \cdots$$

$$F = F_0 + qF_1 + q^2F_3 + \cdots$$

The associated boundary conditions are:

$$w=-1, \quad \theta=1 \quad \text{and} \quad \sigma=1 \quad \text{at} \quad r=r_1,$$

$$w=-1, \quad \theta=0, \quad \text{and} \quad \sigma=0 \quad \text{at} \quad r=r_2=1+\varphi\sin(2\pi z). \tag{12}$$

The initial guess that meets the boundary criteria listed in Equation (13) is:

$$W_{10}=-1-2\pi \in \delta r\cos(2\pi z)+P_o\left[S\ln r+\frac{r^2}{4}+T\right]. \tag{13}$$

Where

$$S=\frac{\left(r_2^2-r_1^2\right)}{4\left(\ln r_1-\ln r_2\right)}, T=\left(\frac{r_1^2\ln r_2-r_2^2\ln r_1}{4\left(\ln r_1-\ln r_2\right)}\right) \text{ and } P_0=\frac{\partial P_0}{\partial z}.$$

By solving Equation (8) and (9) while taking into account the boundary conditions listed in Equation (13), we get the solutions for temperature and concentration profile as follows.

4. Exact solutions of temperature and concentration profile

From Equation (8), we solved the above equations by exact solutions such as:

$$\frac{1}{r}\left(\frac{\partial}{\partial r}\left(r\frac{\partial\sigma}{\partial r}\right)\right)+\frac{N_t}{N_b}\left(\frac{1}{r}\frac{\partial}{\partial r}\left(r\frac{\partial\theta}{\partial r}\right)\right)=0,$$

$$\frac{\partial}{\partial r}\left(r\frac{\partial\sigma}{\partial r}\right)=-\frac{N_t}{N_b}\left(\frac{\partial}{\partial r}\left(r\frac{\partial\theta}{\partial r}\right)\right).$$

Integrating both sides w.r.t "r",

$$r\frac{\partial\sigma}{\partial r}=-\frac{N_t}{N_b}\left(r\frac{\partial\theta}{\partial r}\right)+c_1,$$

$$\sigma=-\frac{N_t}{N_b}\theta+c_1\ln r+c_2. \tag{14}$$

Using Equation (12) for the integration constant values,

$$1=-\frac{N_t}{N_b}+c_1\left(\ln r_1-\ln r_2\right),$$

$$c_1 = \frac{1+\frac{N_t}{N_b}}{(\ln r_1 - \ln r_2)},$$

$$c_2 = -\left(\frac{1+\frac{N_t}{N_b}}{\ln r_1 - \ln r_2}\right)\ln r_2.$$

Entering c_1 and c_2 values in (14),

$$\sigma = -\frac{N_t}{N_b}\theta + h_1(z)\ln r + h_2(z). \tag{15}$$

Where

$$h_1(z) = c_1 = \frac{1+\frac{N_t}{N_b}}{\ln r_1 - \ln r_2} \text{ and } h_2(z) = c_2 = -\left(\frac{1+\frac{N_t}{N_b}}{\ln r_1 - \ln r_2}\right)\ln r_2,$$

$$h_2(z) = c_2 = -h_1(z)\ln r_2.$$

Taking Equation (9),

$$\frac{1}{r}\left(\frac{\partial}{\partial r}\left(r\frac{\partial\theta}{\partial r}\right)\right) + N_b\left(\frac{\partial\theta}{\partial r}\right)\left(\frac{\partial\sigma}{\partial r}\right) - N_t\left(\frac{\partial\theta}{\partial r}\right)^2 = 0.$$

Using Equation (15) for the value of σ,

$$\frac{1}{r}\left(\frac{\partial}{\partial r}\left(r\frac{\partial\theta}{\partial r}\right)\right) = -N_b\left(\frac{\partial\theta}{\partial r}\right)\left(-\frac{N_t}{N_b}\frac{\partial\theta}{\partial r} + h_1(z)\frac{\partial}{\partial r}(\ln r) + \frac{\partial}{\partial r}(h_2(z))\right) - N_t\left(\frac{\partial\theta}{\partial r}\right)^2.$$

Integrating both sides w.r.t "r",

$$r\frac{\partial\theta}{\partial r} = -h_1(z)N_b\theta(r,z) + h_2(z),$$

$$h_2(z) = r\frac{\partial\theta}{\partial r} + N_b h_1(z)\theta(r,z). \tag{16}$$

Let $x = \ln r$, than $\frac{\partial x}{\partial r} = \frac{1}{r}$,

$$e^x = e^{\ln r}, \text{ than } r = e^x,$$

$$\mathscr{L}\{h_2(z)\} = \mathscr{L}\left\{r\frac{\partial\theta}{\partial r} + N_b h_1(z)\theta(x,z)\right\},$$

$$h_2(z)\frac{1}{s} = [s\bar{\theta}(s,z) - \theta(0,z)] + N_b h_1(z)\bar{\theta}(s,z),$$

$$\frac{h_2(z)}{s} = \bar{\theta}(s,z)[s + N_b h_1(z)] - \theta(0,z),$$

$$\bar{\theta}(s,z) = \frac{h_2}{s[s+N_b h_1]} - \frac{\theta(0,z)}{[s+N_b h_1]},$$

$$\mathscr{L}^{-1}\{\bar{\theta}(s,z)\} = \mathscr{L}^{-1}\left\{\frac{h_2}{s(s+N_b h_1)}\right\} + \mathscr{L}^{-1}\left\{\frac{\theta(0,z)}{(s+N_b h_1)}\right\},$$

$$\theta(x,z) = h_2\mathscr{L}^{-1}\left\{\frac{1}{s(s+N_b h_1)}\right\} + \theta(0,z)e^{-N_b h_1 x}. \tag{17}$$

Putting values in Equation (17),

$$\theta(x,z) = h_2\mathscr{L}^{-1}\left\{\frac{1}{sN_b h_1} - \frac{1}{N_b h_1(s+N_b h_1)}\right\} + \theta(0,z)e^{-N_b h_1 x},$$

$$\theta(r,z) = \frac{h_2}{N_b h_1}\left(1 - ((e^x))^{-N_b h_1}\right) + \theta(1,z)((e^x))^{-N_b h_1},$$

$$\theta(r,z) = \frac{h_2}{N_b h_1}\left(1 - (r)^{-N_b h_1}\right) + \theta(1,z)(r)^{-N_b h_1},$$

$$1 = \frac{h_2}{N_b h_1}\left(1 - r_1^{-N_b h_1}\right) + \theta(1,z)r_1^{-N_b h_1},$$

$$1 - \frac{h_2}{N_b h_1} = r_1^{-N_b h_1}\left(-\frac{h_2}{N_b h_1} + \theta(1,z)\right),$$

$$1 - \frac{h_2}{N_b h_1} = r_1^{-N_b h_1}\left(-\frac{h_2}{N_b h_1} + \frac{h_2}{N_b h_1}\left(1 - r_2^{N_b h_1}\right)\right),$$

$$1 = \frac{h_2}{N_b h_1}\left(1 - \left(\frac{r_2}{r_1}\right)^{N_b h_1}\right),$$

$$h_2 = \frac{N_b h_1}{1 - \left(\frac{r_2}{r_1}\right)^{N_b h_1}},$$

$$\theta(r,z)=\frac{1-\left(\frac{r_2}{r}\right)^{N_b h_1}}{1-\left(\frac{r_2}{r_1}\right)^{N_b h_1}},$$

$$\sigma=-\frac{N_t}{N_b}\theta+h_1(z)\ln r+h_2(z),$$

$$\sigma=-\frac{N_t}{N_b}\left[\frac{1-\left(\frac{r_2}{r}\right)^{N_b h_1}}{1-\left(\frac{r_2}{r_1}\right)^{N_b h_1}}\right]+h_1(z)\ln r+h_2(z),$$

$$Ash_2(z)=-h_1(z)\ln r_2,$$

$$\sigma=-\frac{N_t}{N_b}\left[\frac{1-\left(\frac{r_2}{r}\right)^{N_b h_1}}{1-\left(\frac{r_2}{r_1}\right)^{N_b h_1}}\right]+h_1(z)\ln r-h_1(z)\ln r_2,$$

$$\sigma=-\frac{N_t}{N_b}\left[\frac{1-\left(\frac{r_2}{r}\right)^{N_b h_1}}{1-\left(\frac{r_2}{r_1}\right)^{N_b h_1}}\right]+h_1\ln\frac{r}{r_2},$$

$$\theta(r,z)=\frac{1-\left(\frac{r_2}{r}\right)^{N_b h_1}}{1-\left(\frac{r_2}{r_1}\right)^{N_b h_1}}, \tag{18}$$

$$\sigma(r,z)=-\frac{N_t}{N_b}\left[\frac{1-\left(\frac{r_2}{r}\right)^{N_b h_1}}{1-\left(\frac{r_2}{r_1}\right)^{N_b h_1}}\right]+h_1\ln\frac{r}{r_2}. \tag{19}$$

Where $h_1(z)=\frac{1+\frac{N_t}{N_b}}{\ln r_1-\ln r_2}$.

5. Solution for homotopy perturbation

The homotopy perturbation approach is used to get the velocity field and pressure gradient solution. Putting $w=w_0+qw_1+q^2w_2+\cdots$ and $P=P_1+qP_2+q^2P_3+\cdots$ in Equation (11)

$$L(w_0+qw_1+\ q^2w_2+\cdots)$$

$$=L(W_{10})-qL(W_{10})-q\left[\frac{\alpha}{r}\left(\frac{\partial}{\partial r}\left(w_0+qw_1+q^2w_2+\cdots\right)\right)\right.$$

$$+\frac{\beta}{r}\left(\frac{\partial}{\partial r}\left(w_0+qw_1+q^2w_2+\cdots\right)\right)^3+G_r\theta+B_r\sigma$$

$$-M^2\left(\left(w_0+qw_1+q^2w_2+\cdots\right)+1\right)-\frac{\partial}{\partial z}\left(P_1+qP_2+q^2P_3+\cdots\right)\Bigg].$$

After comparing we get these solutions.

5.1 *Zeroth order solution*

$$w_o=-1-2\pi\in\delta r\cos(2\pi z)+P_o\left[S\ln r+\frac{r^2}{4}+T\right] \tag{20}$$

5.2 *First order solution*

$$w_1=-\left(\frac{1}{8}P_0r^2\alpha+\frac{1}{2}P_0S\alpha\log[r]\right)-\left(\frac{1}{8}P_0^3\left(\frac{\left(r^3\right)}{3}+6(r-h)S-\frac{12S^2}{(r)}-\frac{8S^3}{3\left(r^3\right)}\right)\beta\right)$$

$$-\left(-\frac{G\left(r^2\right)\left(-2+h_1N_b+\frac{4\left(\frac{b}{r}\right)^{h_1N_b}}{2-h_1N_b}\right)}{4\left(-1+\left(\frac{b}{a}\right)^{h_1N_b}\right)\left(-2+h_1N_b\right)}\right)-\left(-2rh_1+r\log\left[\frac{r}{b}\right]h_1+\frac{B\left(r^2\right)N_t}{4\left(-1+\left(\frac{b}{a}\right)^{h_1N_b}\right)N_b}\right.$$

$$\left.+\frac{B\left(\frac{b}{r}\right)^{h_1N_b}\left(r^2\right)N_t}{\left(-1+\left(\frac{b}{a}\right)^{h_1N_b}\right)N_b\left(2-h_1N_b\right)\left(-2+h_1N_b\right)}\right)-\left(\frac{1}{64}M^2P_0\left(r^4\right)-\frac{1}{4}M^2P_0\left(r^2\right)S+\frac{1}{4}M^2P_0\left(r^2\right)T\right.$$

$$\left.-\frac{1}{2}M^2\pi\left(r^2\right)\gamma\delta\epsilon\cos[2\pi z]+\frac{1}{4}M^2P_0\left(r^2\right)S\log[r]-\left(\frac{\bar{p}1\left(r^2\right)}{4}\right)\right)+\left(-\frac{1}{-\log[a]+\log[b]}\right)\frac{1}{64}a^4M^2P_0$$

$$-\frac{1}{64}b^4M^2P_0+\frac{a^2\bar{p}1}{4}-\frac{b^2\bar{p}1}{4}-\frac{1}{4}a^2M^2P_0S+\frac{1}{4}b^2M^2P_0S+\frac{1}{4}a^2M^2P_0T-\frac{1}{4}b^2M^2P_0T+\frac{1}{8}a^2P_0\alpha$$

$$-\frac{1}{8}b^2P_0\alpha+\frac{1}{8}{P_0}^3\left(\frac{a^3}{3}+6(a-h)S-\frac{12S^2}{a}-\frac{8S^3}{3a^3}\right)\beta-\frac{1}{8}{P_0}^3\left(\frac{b^3}{3}+6(b-h)S-\frac{12S^2}{b}-\frac{8S^3}{3b^3}\right)\beta$$

$$+4\pi\bar{z}\pi\epsilon\delta\gamma\cos-\frac{1}{2}a^2M^2\pi\gamma\delta\epsilon\cos[2\pi z]+\frac{1}{2}b^2M^2\pi\gamma\delta\epsilon\cos[2\pi z]+\frac{1}{4}a^2M^2P_0S\log[a]$$

$$+\frac{1}{2}P_0S\alpha\log[a]-P_0\left(\frac{a^2}{4}+T+S\log[a]\right)-\frac{1}{4}b^2M^2P_0S\log[b]-\frac{1}{2}P_0S\alpha\log[b]$$

$$+P_0\left(\frac{b^2}{4}+T+S\log[b]\right)-2ah_1+2bh_1+a\log\left[\frac{a}{b}\right]h_1 \tag{21}$$

Adding Equations (20) and (21), the solutions for velocity field can be written as for $q=1$:

$$w=w_0+qw_1+\cdots$$

$$w=-1-2\pi\in\delta r\cos(2\pi z)+P_o\left[S\ln r+\frac{r^2}{4}+T\right]=-\left(\frac{1}{8}P_0r^2\alpha+\frac{1}{2}P_0S\alpha\log[r]\right)$$

$$-\left(\frac{1}{8}P_0^3\left(\frac{(r^3)}{3}+6(r-h)S-\frac{12S^2}{(r)}-\frac{8S^3}{3(r^3)}\right)\beta\right)-\left(-\frac{G\left(r^2\right)\left(-2+h_1N_b+\frac{4\left(\frac{b}{r}\right)^{h_1N_b}}{2-h_1N_b}\right)}{4\left(-1+\left(\frac{b}{a}\right)^{h_1N_b}\right)(-2+h_1N_b)}\right)-\Bigg(-2rh_1$$

$$+r\log\left[\frac{r}{b}\right]h_1+\frac{B\left(r^2\right)N_t}{4\left(-1+\left(\frac{b}{a}\right)^{h_1N_b}\right)N_b}+\frac{B\left(\frac{b}{r}\right)^{h_1N_b}\left(r^2\right)N_t}{\left(-1+\left(\frac{b}{a}\right)^{h_1N_b}\right)N_b(2-h_1N_b)(-2+h_1N_b)}\Bigg)-\Bigg(\frac{1}{64}M^2P_0\left(r^4\right)$$

$$-\frac{1}{4}M^2P_0\left(r^2\right)S+\frac{1}{4}M^2P_0\left(r^2\right)T-\frac{1}{2}M^2\pi\left(r^2\right)\gamma\delta\epsilon\cos[2\pi z]+\frac{1}{4}M^2P_0\left(r^2\right)S\log[r]-\left(\frac{\bar{p}1\left(r^2\right)}{4}\right)\Bigg)$$

$$+\Bigg(-\frac{1}{-\log[a]+\log[b]}\Bigg(\frac{1}{64}a^4M^2P_0-\frac{1}{64}b^4M^2P_0+\frac{a^2\bar{p}1}{4}-\frac{b^2\bar{p}1}{4}-\frac{1}{4}a^2M^2P_0S+\frac{1}{4}b^2M^2P_0S$$

$$+\frac{1}{4}a^2M^2P_0T-\frac{1}{4}b^2M^2P_0T+\frac{1}{8}a^2P_0\alpha-\frac{1}{8}b^2P_0\alpha+\frac{1}{8}P_0^3\left(\frac{a^3}{3}+6(a-h)S-\frac{12S^2}{a}-\frac{8S^3}{3a^3}\right)\beta$$

$$-\frac{1}{8}P_0^3\left(\frac{b^3}{3}+6(b-h)S-\frac{12S^2}{b}-\frac{8S^3}{3b^3}\right)\beta+4\pi\bar{z}\pi\epsilon\delta\gamma\cos-\frac{1}{2}a^2M^2\pi\gamma\delta\epsilon\cos[2\pi z]$$

$$+\frac{1}{2}b^2M^2\pi\gamma\delta\epsilon\cos[2\pi z]+\frac{1}{4}a^2M^2P_0S\log[a]+\frac{1}{2}P_0S\alpha\log[a]-P_0\left(\frac{a^2}{4}+T+S\log[a]\right)$$

$$-\frac{1}{4}b^2M^2P_0S\log[b]-\frac{1}{2}P_0S\alpha\log[b]+P_0\left(\frac{b^2}{4}+T+S\log[b]\right)-2ah_1+2bh_1+a\log\left[\frac{a}{b}\right]h_1\cdots \tag{22}$$

The frictional force F and pressure rise $\Delta\bar{P}$ on the inner and outer pipes F_0, F_1 are calculated by:

$$\Delta P=\int_0^1\frac{dP}{dz}dz, \tag{23}$$

$$F_0 = \int_a^b r\left(-1 - 2\pi\epsilon\delta\gamma\cos[2\pi z] + \left(S\log[r] + \frac{r^2}{4} + T\right)P_0\right)dr, \tag{24}$$

$$F_1 = \int_0^h r\left(-\left(\frac{r^2-h^2}{4}\right)P_0 + \left(\frac{r^2-h^2}{4}\right)P_1 - \left(\frac{1}{32}P_0^3\left(r^4-h^4\right)\alpha_1\alpha_2\right) - \left(\frac{1}{192}P_0^5\left(r^6-h^6\right)\alpha_3{\alpha^2}_1\right)\right.$$

$$+\left(\frac{1}{16}Gh^2\left(r^2-h^2\right)\right) - \left(\frac{G\left(r^4-h^4\right)}{64}\right) + \left(\frac{Bh^2\left(r^2-h^2\right)N_t}{16N_b}\right) - \left(\frac{B\left(r^4-h^4\right)N_t}{64N_b}\right)$$

$$\left.-\left(\frac{1}{16}h^2M^2P_0\left(r^2-h^2\right)\right) + \left(\frac{1}{64}M^2P_0\left(r^4-h^4\right)\right) - \left(\frac{1}{2}M^2\pi\left(r^2-h^2\right)\alpha\delta\epsilon\cos[2\pi z]\right)\right)dr. \tag{25}$$

Where $\frac{dP}{dz}$ is defined in Equation (23).
In dimensionless form, flow rate can be expressed as:

$$F_0 = \frac{a^2}{2} - \frac{b^2}{2} + a^2\pi\gamma\delta\epsilon\cos[2\pi z] - b^2\pi\gamma\delta\epsilon\cos[2\pi z] + \bar{P}_0\left(-\frac{a^4}{16} + \frac{b^4}{16} - \frac{a^2T}{2} + \frac{b^2T}{2}\right.$$

$$\left.+ S\left(-\frac{1}{4}a^2(-1+2\log[a]) + \frac{1}{4}b^2(-1+2\log[b])\right)\right), \tag{26}$$

$$F_1 = -\frac{Gh^6}{96} + \frac{h^4P_0}{16} + \frac{1}{96}h^6M^2P_0 - \frac{h^4P_1}{16} + \frac{1}{8}h^4M^2\pi\alpha\delta\epsilon\cos[2\pi z] - \frac{Bh^6N_t}{96N_b} + \frac{1}{96}h^6P_0^3\alpha_1\alpha_2$$

$$+\frac{1}{512}h^8P_0^5\alpha_3\alpha_1^2, \tag{27}$$

$$F = F_0 + F_1,$$

$$F = \frac{a^2}{2} - \frac{b^2}{2} + a^2\pi\gamma\delta\epsilon\cos[2\pi z] - b^2\pi\gamma\delta\epsilon\cos[2\pi z] + \bar{P}_0\left(-\frac{a^4}{16} + \frac{b^4}{16} - \frac{a^2T}{2} + \frac{b^2T}{2}\right.$$

$$\left.+ S\left(-\frac{1}{4}a^2(-1+2\log[a]) + \frac{1}{4}b^2(-1+2\log[b])\right)\right) - \frac{Gh^6}{96} + \frac{h^4P_0}{16} + \frac{1}{96}h^6M^2P_0 - \frac{h^4P_1}{16}$$

$$+\frac{1}{8}h^4M^2\pi\alpha\delta\epsilon\cos[2\pi z] - \frac{Bh^6N_t}{96N_b} + \frac{1}{96}h^6P_0^3\alpha_1\alpha_2 + \frac{1}{512}h^8P_0^5\alpha_3{\alpha^2}_1. \tag{28}$$

The following terms can be used to define the pressure gradient:

$$\frac{dP}{dz} = -\frac{16}{h^4}\left(F + \frac{h^2}{2} + h^2\pi\alpha\delta\epsilon\cos[2\pi z] + \left(\frac{Gh^6}{96} - \frac{h^4\bar{P}_0}{16} - \frac{1}{96}h^6M^2\bar{P}_0 - \frac{1}{8}h^4M^2\pi\alpha\delta\epsilon\cos[2\pi z]\right.\right.$$

$$+\frac{Bh^6N_t}{96N_b}-\frac{1}{96}h^6\bar{P}_0^3\alpha_1\alpha_2-\frac{1}{512}h^8\bar{P}_0^5\alpha_3\alpha_1^2\Bigg)\Bigg).$$

Stream functions define velocities as follows:

$$u=\frac{-1}{r}\left(\frac{\partial\Psi}{\partial z}\right)\quad\text{and}\quad w=\frac{1}{r}\left(\frac{\partial\Psi}{\partial r}\right).$$

The solution of the stream function can be written as:

$$\begin{aligned}\psi=&-\frac{r^2}{2}-\frac{3}{128}Gh^4r^2-\frac{1}{8}h^2Pr^2+\frac{3}{128}h^4M^2P_0r^2+\frac{1}{64}Gh^2r^4+\frac{Pr^4}{16}-\frac{1}{64}h^2M^2P_0r^4-\frac{Gr^6}{384}\\&+\frac{1}{384}M^2P_0r^6-\pi r^2\alpha\delta\epsilon\cos[2\pi z]+\frac{1}{4}h^2M^2\pi r^2\alpha\delta\epsilon\cos[2\pi z]-\frac{1}{8}M^2\pi r^4\alpha\delta\epsilon\cos[2\pi z]\\&-\frac{3Bh^4r^2N_t}{128N_b}+\frac{Bh^2r^4N_t}{64N_b}-\frac{Br^6N_t}{384N_b}+\frac{1}{64}h^4{P_0}^3r^2\alpha_1\alpha_2-\frac{1}{192}{P_0}^3r^6\alpha_1\alpha_2+\frac{1}{384}h^6{P_0}^5r^2\alpha_3{\alpha^2}_1\\&-\frac{{P_0}^5r^8\alpha_3{\alpha^2}_1}{1536}.\end{aligned}\tag{29}$$

5.3 *Limitations*

The study examined two-dimensional laminar flow of a Newtonian base fluid with constant viscosity that is independent of temperature, which may diminish its practical relevance. While the 2D flow assumption simplifies the model, it fails to account for three-dimensional effects that
occur in complex geometries typical of real bio-convective systems. By restricting the analysis to laminar flow, the study overlooks potential turbulent interactions that can arise in high-velocity MHD nanofluid conditions. Furthermore, the assumption of a Newtonian base fluid disregards the non-Newtonian characteristics commonly found in biological fluids, which may compromise the accuracy of analyses regarding ciliary-driven transport. Additionally, neglecting temperature-dependent viscosity may result in an underestimation of thermal effects in heat transfer applications.

6. Results and discussions

We solved the governing equation and developed the results in graphical form. We debated the mechanical behavior characterizations of a non-Newtonian Prandtl fluid in a vertical endoscopy tube when the effects of the following parameters for the problem are fluid parameter, magnetohydrodynamics, Grashof number, thermophoresis parameter, Brownian motion, Brinkman number, inner tube radius and amplitude ratio. Figures 2–5 show the effects of temperature profile and concentration. Figures 2–3 illustrate how the temperature profile increases as the magnitudes of N_t and N_b in the base fluid increase. According to these graphs, the temperature peaks close to the tube's outside edge. In conclusion, graphs explain that both parameters shed light on how particles behave inside a fluid. The thermophoretic parameter concentrates on the impacts of temperature gradients, while the Brownian parameter focuses on the consequences of arbitrary thermal movement. Thermophoresis and Brownian motion arise from the thermophoretic force that drives nanoparticles from the hot region toward the cooler region. The results enhanced the thermal boundary layer thickness and increased the fluid

temperature. The curve indicated that stronger thermophoretic effects promoted better heat distribution within the fluid. The concentration profile is illustrated in Figures 4–5. The concentration profile increased with rising N_b in the base fluid and decreased with increasing N_t. We concluded that as N_b increased, the distribution of nanoparticles in the base fluid also increased while the concentration profile decreased with the influence of N_t. The motion of the particles is influenced by the random thermal movement of the fluid molecules. Figures 6–9 show the velocity profile variations caused by the various components of the issue. Figures 6–7 revealed the impacts of thermophoresis and magnetic field on the velocity profile amplitude. The increase in the thermophoresis parameter leads to a reduction in the amplitude of the velocity profile. The fluid decelerates with increasing N_t, indicating that stronger thermal-particle interactions are resisting the flow.

The trend indicates that thermophoretic forces influence momentum transfer by reducing flow velocity near the peaks and troughs of the wave. A rise in the magnetic parameter M (magnetohydrodynamic effect) decreases velocity throughout the domain. Magnetic force created a Lorentz drag that opposed motion which is reflected in the reduced peak velocities. Such a type of damping effect becomes more pronounced at higher values of the magnetic parameter M which highlights the resistance of the magnetic field conducting in nanofluid. Figures 7–8 illustrated that the velocity profile decreased as the effects of the amplitude ratio φ diminished. An increase in the magnitude of the variables B and N led to a rise in velocity at every location within the zone. As depicted in Figure 9, the velocity profile increased with rising Grashof number. The figure indicated that buoyancy forces significantly influence the region $r \in [0.6, 1.4]$ which resulted in a increase in the velocity profile with higher Gr values. Increased internal heat generation raised the fluid temperature which altered the buoyancy force and modified momentum. The resulting thermal energy induced greater fluid resistance. Stronger thermal gradients promoted flow acceleration.

Figures 10–13 illustrate the properties of the pressure gradient dP/dz for various wave forms and different types of waves. Figure 10 illustrates that as the thermophoresis parameter (N_t) increased, the pressure gradient profile exhibited a higher peak. The stronger thermophoretic forces contributed to increasing pressure buildup along the channel. Figure 11 indicated that larger values of the geometry/stretching parameter (b) led to a significant increase in the peak of the pressure gradient. This rise in pressure gradient peak implied that geometric stretching enhanced resistance in the axial direction. Figure 12 presents the impact of Brownian motion on pressure variation. Increasing the Brownian motion parameter N_b led to an increase in pressure variation. Brownian diffusion effects strengthen local pressure fluctuations which enhance the momentum exchange. Figure 13 illustrates thermophoresis effects on the pressure gradient. An increase in N_t led to more pronounced spikes in the pressure gradient. The thermophoresis induces localized steep pressure changes. A bolus moves at the speed of a wave and progresses through the peristaltic wave in a process known as trapping. A bolus becomes entrapped by expanded streamlines within the wave frame. Figures 14–16 displayed the streamlines for square, triangular, trapezoidal, sinusoidal and multi-sinusoidal waves. These graphs demonstrated that bolus size decreased in triangle waves when compared to other waves.

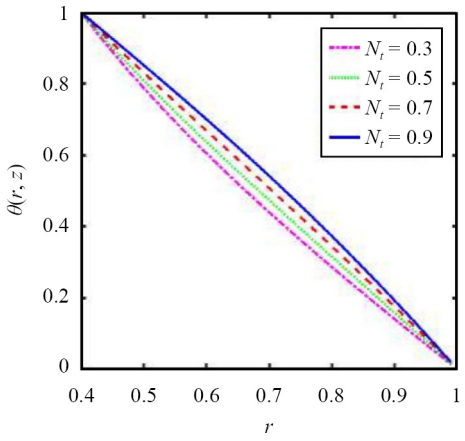

Figure 2. Temperature profile for N_t, $z = 0.9$, $\varphi = 1.2$, $r_1 = 1.1$ and $N_b = 1.35$

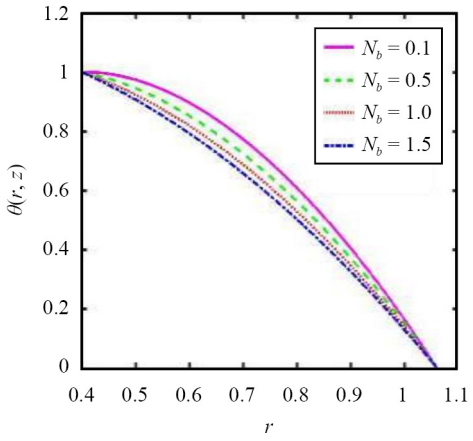

Figure 3. Temperature profile for N_b, $z = 1.6$, $\varphi = 1.11$, $r_1 = 0.2$ and $N_t = 0.88$

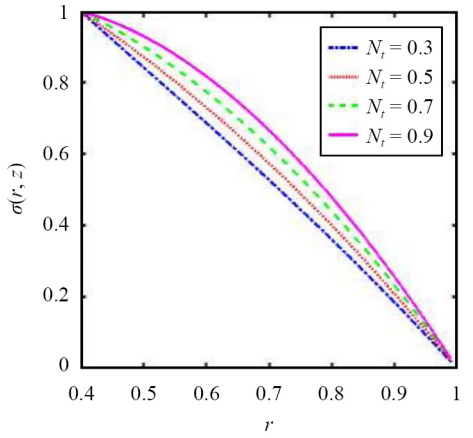

Figure 4. Concentration profile for N_t, $z = 1.6$, $\varphi = 1.11$, $r_1 = 0.2$ and $N_b = 0.88$

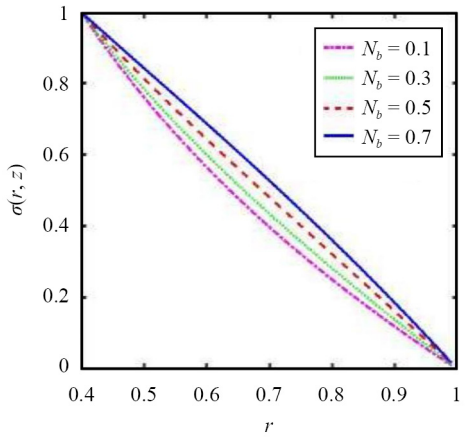

Figure 5. Concentration profile for N_b, $z = 1.6$, $\varphi = 1.11$, $r_1 = 0.2$ and $N_t = 0.88$

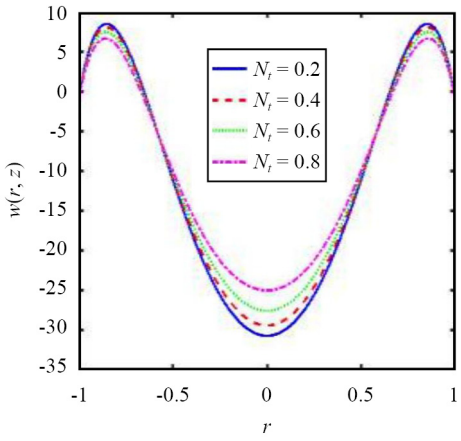

Figure 6. Velocity profile for N_t, $z = 0.8$, $\varphi = 2.9$, $r_1 = 0.2$, $M = 1.9$, $b = -0.7$, $B_r = 4$, $N_b = 1.5$, $G_r = 1.22$

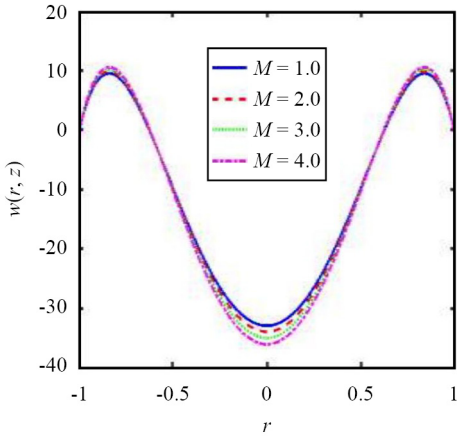

Figure 7. Velocity profile for M, $z = 1.02$, $\varphi = 1.1$, $r_1 = 1.3$, $N_t = -1.0$, $b = -0.7$, $N_b = 1.2$, $G_r = 0.01$, $B_r = 1.2$

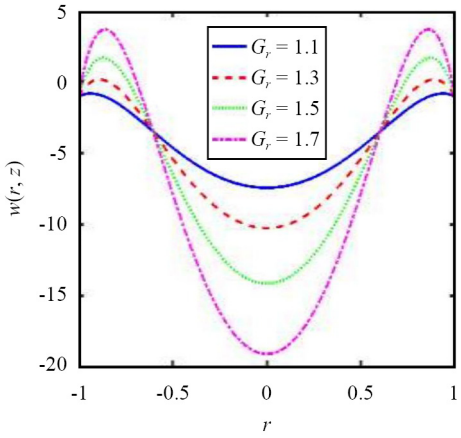

Figure 8. Velocity profile for G_r, $z = 0.75$, $B_r = 1.2$, $r_1 = 0.4$, $M = -1.5$, $b = -0.7$, $N_t = 4$, $N_b = 3.4$, $r_1 = 0.01$

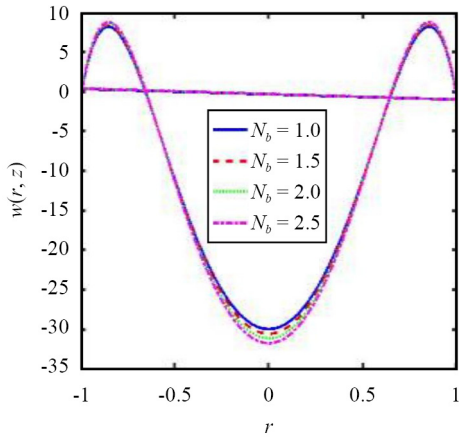

Figure 9. Velocity profile for N_b, $z = 1.02$, $\varphi = 1.1$, $r_1 = 1.3$, $M = -1.0$, $b = -0.7$, $G_r = 1.2$, $N_t = 0.01$, $B_r = 0.02$

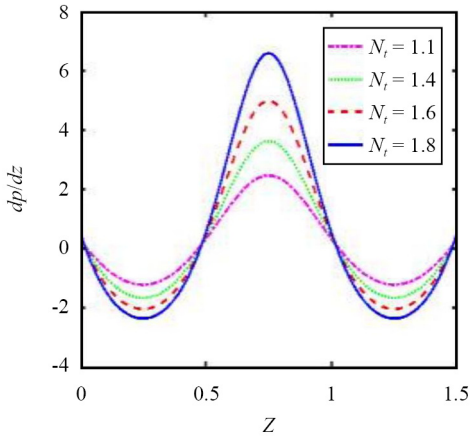

Figure 10. Pressure gradient for N_t, $b = 1.2$, $\theta = 0.2$, $\varphi = 1.01$, $N_b = 1.2$, $G_r = 4.5$, $B_r = 1.1$, $M = -10$, $r_1 = 0.05$

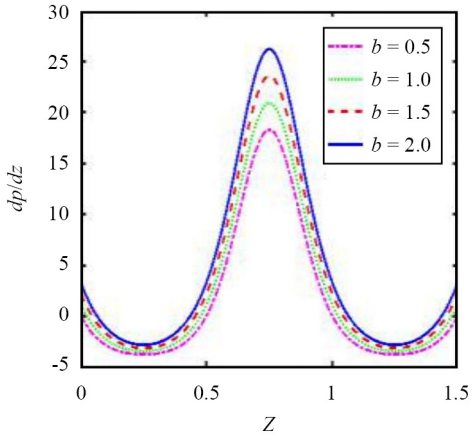

Figure 11. Pressure gradient for b, $\theta = 1.2$, $r_1 = 1.44$, $N_t = 1.1$, $N_b = 0.2$, $G_r = 4.5$, $B_r = 1.1$ and $M = -10$

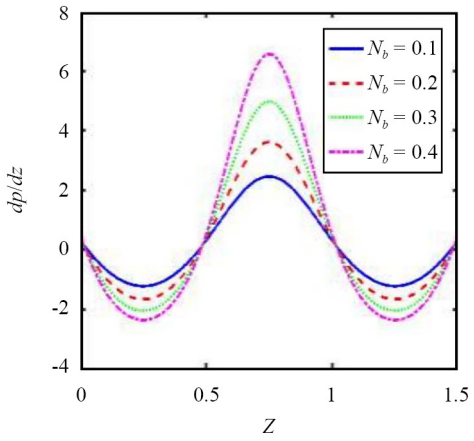

Figure 12. Pressure gradient for N_b, $\theta = 0.1$, $\varphi = 0.11$, $N_t = 0.1$, $r_1 = 0.04$, $b = 1.1$, $G_r = 5$, $B_r = 1.0$, $M = 1.1$

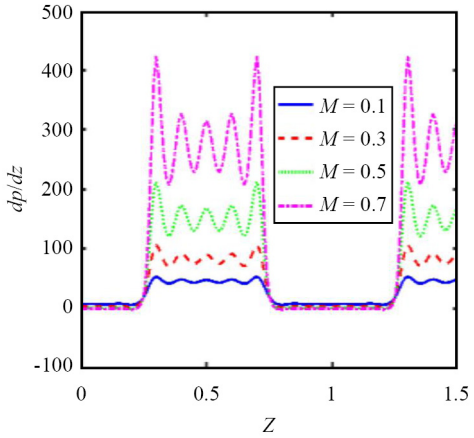

Figure 13. Pressure gradient for r_1, $N_t = 0.1$, $\theta = 1.2$, $\varphi = 0.9$, $b = 1$, $G_r = 4.5$, $B_r = 1.1$, $N_b = 1.2$

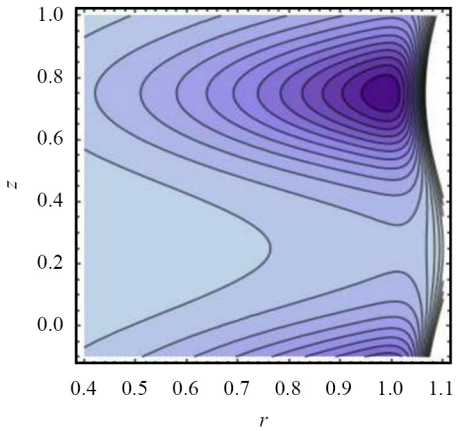

Figure 14. Streamline for sinusoidal wave

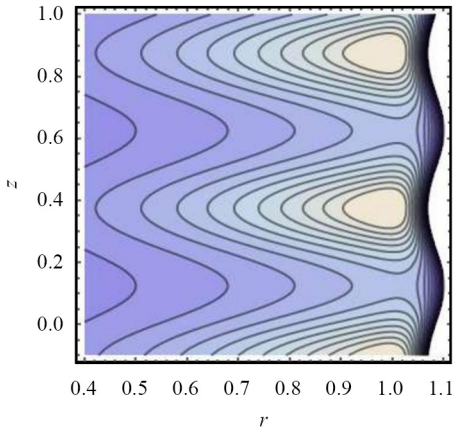

Figure 15. Streamline for multisinusoidal wave

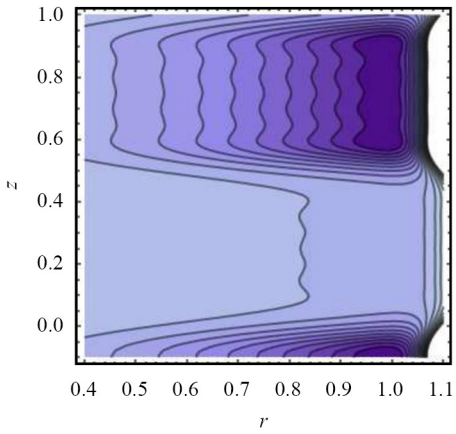

Figure 16. Streamline for square wave, $r_1 = 0.50$, $G_r = -1.7$, $\theta = -0.2$, $M = 1.1$, $N_b = 2$, $b = -3.00$, $\varphi = 1.2$, $B_r = 2$ and $N_t = 6$

7. Conclusion

Our research focused on peristaltic transport of Prandtl nanofluid specifically examining the combined effects of heat transfer and MHD. Key findings include:

- Precise control of nanofluid flow facilitated ciliary oscillation along with MHD force which enhanced the fluid propulsion and particle dispersion for targeted medicinal intervention.
- The temperature gradient increases in steepness with higher N_t and particle movement under the temperature gradient enhances heat transfer.
- The influence of N_b is more pronounced near the boundary which indicates a greater level of nanoparticle agitation and enhanced energy transport.
- Thermophoresis and Brownian motion play a significant role in influencing the internal pressure distribution as a result of nanoparticle movement.
- The trapping bolus size of the triangular wave is smaller compared to other wave types.

Acknowledgement

The authors would like to thank Prince Sultan University for their support through the TAS research lab.

Conflict of interest

The authors state that they have no financial interests or personal relationships that could have influenced the work presented in this paper.

References

[1] Fatima I, Asghar S. Imposed pressure driven flow in peristalsis. *Advances in Mechanical Engineering*. 2020; 12(11): 1687814020971063.

[2] Tanveer A, Khan M, Salahuddin T, Malik MY, Khan F. Theoretical investigation of peristaltic activity in MHD based blood flow of non-Newtonian material. *Computer Methods and Programs in Biomedicine*. 2020; 187: 105225.

[3] Javid K, Asghar Z, Rehman FU. Biomechanics of electro-kinetically modulated peristaltic motion of bio-fluid through a divergent complex wavy channel. *Canadian Journal of Physics*. 2021; 99(2): 70–79.

[4] Elboughdiri N, Javid K, Ahmed I, Naz H, Khan SU, Salih AA, et al. Peristaltic pumping of hybrid nanofluid between concentric tubes with magnetic device effects: Applications to human endoscopy. *Journal of the Indian Chemical Society*. 2022; 99(10): 100710.

[5] Devakar M, Ramesh K, Vajravelu K. Magnetohydrodynamic effects on the peristaltic flow of couple stress fluid in an inclined tube with endoscope. *Journal of Computational Mathematics and Data Science*. 2022; 2: 100025.

[6] Asha SK, Talawar VT, Bhatti MM. Entropy generation and radiation analysis on peristaltic transport of hyperbolic tangent fluid with hybrid nanoparticle through an endoscope. *Journal of Nanofluids*. 2023; 12(3): 723–737.

[7] Jawad M, Shah Z, Islam S, Khan W, Khan AZ. Nanofluid thin film flow of Sisko fluid and variable heat transfer over an unsteady stretching surface with external magnetic field. *Journal of Algorithms and Computational Technology*. 2019; 13: 1748301819832456.

[8] McCash LB, Zehra I, Al-Zubaidi A, Amjad M, Abbas N, Nadeem S. Combined effects of binary chemical reaction/activation energy on the flow of Sisko fluid over a curved surface. *Crystals*. 2021; 11(8): 967.

[9] Shaheen A, Asjad MI. Peristaltic flow of a Sisko fluid over a convectively heated surface with viscous dissipation. *Journal of Physics and Chemistry of Solids*. 2018; 122: 210–217.

[10] Mumtaz F, Al-Zubaidi A, Abbas T, Saleem S. Thermal performance analysis of quaternary hybrid nanofluids with radiative and Joule heating effects in magnetohydrodynamic flow over a stretched surface. *Results in Physics*. 2025; 71: 108176.

[11] Alharbi W, Aljohani A, El-Zahar E, Ebaid A. Exact solution of non-Newtonian blood flow with nanoparticles through porous arteries: A comparative study. *Computers, Materials and Continua*. 2020; 63(3): 1143–1157.

[12] Kumar MD, Raju CS, Sajjan K, Dharmaiah G, Shah NA, Yook SJ. Artificial neural networks for mass transfer and bioconvection analysis in radiative Eyring-Powell flow over a convective cylinder surface: Application to microbial fuel cells. *Engineering Applications of Artificial Intelligence*. 2025; 156: 111256.

[13] Arshad M. MHD hybrid nanofluid flow in a rotating system with an inclined magnetic field and thermal radiation. *Case Studies in Thermal Engineering*. 2024; 62: 105182.

[14] Ayub A, Shah SZ, Asjad MI, Almusawa MY, Eldin SM, El-Rahman MA. Biological interactions between micro swimmers and cross fluid with inclined MHD effects in a complex wavy canal. *Scientific Reports*. 2023; 13(1): 4712.

[15] Tanveer A, Ashraf MB. Mixed convective flow of Sisko nanofluids over a curved surface with entropy generation and Joule heating. *Arabian Journal for Science and Engineering*. 2023; 48(9): 11263–11275.

[16] Bahnasy A, Abdel-Wahab AM. Mathematical model represents the effect of flexible endoscopy on suspension fluid flow. *Journal of Advanced Research in Fluid Mechanics and Thermal Sciences*. 2022; 89: 42–61.

[17] Rafiq M, Shaheen A, Trabelsi Y, Eldin SM, Khan MI, Suker DK. Impact of activation energy and variable properties on peristaltic flow through porous wall channel. *Scientific Reports*. 2023; 13(1): 3219.

[18] Abbas Z, Rafiq MY, Hasnain J, Javed T. Peristaltic transport of a Casson fluid in a non-uniform inclined tube with Rosseland approximation and wall properties. *Arabian Journal for Science and Engineering*. 2021; 46(3): 1997–2007.
[19] Hafez NM, Abd-Alla AM, Metwaly TM. Influences of rotation and mass and heat transfer on MHD peristaltic transport of Casson fluid through inclined plane. *Alexandria Engineering Journal*. 2023; 68: 665–692.
[20] Mahendra DL, Viharika JU, Ramanjini V, Makinde OD, Vishwanatha UB. Entropy analysis on the bioconvective peristaltic flow of gyrotactic microbes in Eyring-Powell nanofluid through an asymmetric channel. *Journal of the Indian Chemical Society*. 2023; 100(3): 100935.
[21] Abdelhafez MA, Abd-Alla AM, Abo-Dahab SM, Elmhedy Y. Influence of an inclined magnetic field and heat and mass transfer on the peristaltic flow of blood in an asymmetric channel. *Scientific Reports*. 2023; 13(1): 5749.
[22] Alhazmi SE, Imran A, Awais M, Abbas M, Alhejaili W, Hamam H, et al. Thermal convection in nanofluids for peristaltic flow in a nonuniform channel. *Scientific Reports*. 2022; 12(1): 12412.
[23] Fatima N, Saidani T, Ijaz N, Saleem N, Zeeshan A. Thermal energy and electro-osmotic influences for biomimetic artificial olfactory cilia in tri-hybrid nanofluids. *Nanotechnology*. 2024; 35(47): 475402.
[24] Asghar Z, Khalid U, Nazeer M, Rasheed HS, Kausar A. Computational study of flow and heat transfer analysis of Ellis fluid model in complicated divergent channel. *Modern Physics Letters B*. 2024; 38(14): 2450119.
[25] Sadaf H, Asghar Z, Ijaz S. Mathematical modeling of Cross-fluid model in a peristaltic channel with viscous dissipation and MHD effects. *ZAMM–Journal of Applied Mathematics and Mechanics*. 2024; 104(6): e202300334.
[26] Asghar Z, Shah RA, Waqas M, Gondal MA. Electro-fluid-dynamics (EFD) of soft-bodied organisms swimming through mucus having dilatant, viscous, and pseudo-plastic properties. *International Journal of Modern Physics B*. 2025; 39(1): 2550011.